**Atmospheric
Measurement
Techniques
Discussions**

Retrieval of tropospheric CO column from hyperspectral infrared sounders – application to four years of Aqua/AIRS and MetOp-A/IASI

T. Thonat[1], C. Crevoisier[1], N. A. Scott[1], A. Chédin[1], T. Schuck[2], R. Armante[1], and L. Crépeau[1]

[1]Laboratoire de Météorologie Dynamique, CNRS, IPSL – UMR8539, Ecole Polytechnique, Palaiseau, France
[2]Atmospheric Chemistry Division, Max Planck Institute for Chemistry, Mainz, Germany

Title Page	
Abstract	Introduction
Conclusions	References
Tables	Figures
◄◄	►►
◄	►
Back	Close
Full Screen / Esc	
Printer-friendly Version	
Interactive Discussion	

Abstract

Four years of tropospheric integrated content of CO are retrieved from infrared hyper-spectral observations of AIRS onboard Aqua and IASI onboard MetOp-A, for the period July 2007–June 2011. The retrieval method is based on a double differential approach that relies on the difference between brightness temperatures (BT) observed by the sounder and BT simulated by the 4A radiative transfer model on collocated ECMWF reanalyses, for several couples of channels located in the 4.7 µm CO band. AIRS and IASI give access to similar integrated contents of CO with a maximum sensitivity near 450 hPa and half a maximum between 200 and 750 hPa depending on the thermal contrast (i.e. the difference between the surface temperature and the temperature of the first pressure level). However, differences in their spectral and radiometric characteristics yield differences in the retrieval characteristics with AIRS selected couples of channels being more sensitive to surface characteristics. Moreover, IASI covers the whole CO absorption band, with a 3 times greater spectral resolution, giving access to channels presenting a 3 times higher signal to noise ratio. This results in a better precision and lower standard deviation of the IASI retrievals. Conservatively, comparisons with CARIBIC aircraft measurements yield a relative difference of 3.42 % for IASI and 4.92 % for AIRS. On average, AIRS and IASI retrievals are in very good agreement, showing the same seasonality, seasonal amplitudes, interannual variability and spatial distribution. The analysis of the monthly evolution of CO particularly highlights the strong influence of biomass burning on the evolution of CO in several tropical regions. In particular, a sharp increase in CO in 2010 in the southern tropics, especially over South America and South Africa, is observed, and is shown to be related to El Niño and to the Atlantic Multidecadal Oscillation.

Full Screen / Esc

Printer-friendly Version

Interactive Discussion

Application to four years of Aqua/AIRS and MetOp-A/IASI

T. Thonat et al.

1 Introduction

Carbon monoxide (CO) is produced by the combustion of fossil fuel, biomass burning, and the oxidation of biogenic hydrocarbons and methane. At northern midlatitudes, the main source is fossil fuel combustion, while in the tropics the three other sources prevail. In addition to being an air pollutant, its removal by OH, which also reacts with methane, halocarbons and ozone, makes CO an important gas by indirectly influencing greenhouse gases, and having a significant impact on air quality. CO has a lifetime ranging from 10 days in the tropics in summer to more than a year over the poles in winter. Thanks to its relatively long atmospheric lifetime, CO also serves as a tracer of long-range transport of pollution, and plays a key role in the understanding of the biomass burning issue. For all these reasons, an accurate monitoring of CO is essential to better understand the spatiotemporal variability of CO sources and sinks (Holloway et al., 2000; Duncan et al., 2007).

Ground-based accurate measurements of CO are available (e.g. from the World Data Centre for Greenhouse Gases; WMO, 2009), but they are quite sparse, and mainly concentrated in Europe and North America. Aircraft measurements also provide data on CO (e.g. the MOZAIC, CARIBIC and CONTRAIL programs; Nedelec et al., 2003; Brenninkmeijer et al., 2007; Machida et al., 2008), but are limited in time and space. As a consequence, CO observations from space have been used in recent years to get a global coverage. The first space borne instrument to monitor CO was the Measurement Atmospheric Pollution from Space (MAPS), which flew onboard the Space Shuttle for a few days in 1981, 1984 and 1994 (Reichle et al., 1999). It was followed by the Interferometric Monitor for Greenhouse gases instrument (IMG) that operated between October 1996 and June 1997 (Clerbaux et al., 1999). Over the past decade, several nadir viewing instruments have been measuring tropospheric CO with a greater spatial and temporal coverage, including the Measurements of Pollution in the Troposphere instrument (MOPITT, launched in March 2000; Deeter et al., 2003, 2009), the Atmospheric Infrared Sounder (AIRS, launched in May 2002; McMillan et al., 2005),

the Scanning Imaging Absorption Spectrometer for Atmospheric Chartography (SCIA-MACHY, launched in March 2002; Buchwitz et al., 2004; Frankenberg et al., 2005; de Laat et al., 2006) and the Tropospheric Emission Spectrometer (TES, launched in July 2004; Rinsland et al., 2006). With the exception of SCIAMACHY, which measures
5 the scattered, reflected and transmitted near-infrared solar radiation, giving access to the full CO column, these instruments are thermal infrared sounders, thus mostly sensitive to CO in the mid-troposphere. These instruments have stressed the great value of infrared observation of CO from space, by providing a better constraint on top-down flux inversions (e.g. Kopacz et al., 2010; Fortems-Cheiney et al., 2011), and by giving
10 valuable information on specific signals such as fire emissions (Edwards et al., 2004; Yurganov et al., 2008), pollution events (Turquety et al., 2008) or the impact of El Niño (Rinsland et al., 2008).

With its 8461 channels covering most of the infrared spectrum at a very high resolution, the Infrared Sounding Interferometer (IASI) was launched in October 2006
15 onboard the European MetOp-A platform, and is operational since July 2007. Like the AIRS instrument, it has been designed to provide water vapour and temperature soundings for operational meteorology, as well as to observe simultaneously the most important trace gases (Hilton et al., 2012). Some studies have already highlighted the suitability of IASI to measure CO from space (Turquety et al., 2009; George et al.,
20 2009; Illingworth et al., 2011). These studies presented estimations of CO based on optimal estimation techniques. Here, we use an alternative approach for the retrieval of a tropospheric integrated content of CO, that relies on differences between simulated and observed radiances from AIRS and IASI, and that allows us to study the characteristics of the retrieved CO stemming from the spectral and radiometric characteristics
25 of the sounders. Our study focuses on the tropics, where strong fire CO emissions are located. Section 2 describes the data and modelling tools used in the retrieval process. Section 3 presents the selection of AIRS and IASI channels based on their sensitivity to CO and other atmospheric and surface variables, and the method used to retrieve CO with these channels. Section 4 presents the results, comparisons with CARIBIC

measurements and analysis of the retrieved CO in terms of geographic distribution and monthly evolution in light of fire activity and climate indexes. Section 5 concludes this study.

2 Data and models

2.1 AIRS

The Atmospheric Infrared Sounder (AIRS) is a polar-orbiting nadir-viewing instrument. It was launched onboard the Aqua satellite in May 2002, and is operational since September 2002. With its 2378 channels, its spectral domain ranges from $650\,\mathrm{cm}^{-1}$ to $2665\,\mathrm{cm}^{-1}$ (15.4 µm and 3.8 µm), with a resolving power ($\lambda/\Delta\lambda$) of 1200 (i.e. a spectral resolution ranging from $0.5\,\mathrm{cm}^{-1}$ to $2\,\mathrm{cm}^{-1}$). This domain is divided into three spectral bands, from 650 to $1135\,\mathrm{cm}^{-1}$, from 1215 to $1615\,\mathrm{cm}^{-1}$ and from 2180 to $2665\,\mathrm{cm}^{-1}$. AIRS cross-track scanning is 1650 km and covers 70 % of the earth every day. The instantaneous field of view (IFOV) is sampled by 3×3 circular pixels whose ground resolution is 13 km at nadir. In this study, use is made of the Version 5 Level 1b data (available at http://mirador.gsfc.nasa.gov/). Also flying onboard Aqua, the Advanced Microwave Sounding Unit (AMSU) observations are used in this study for cloud detection.

2.2 IASI

The Infrared Atmospheric Sounding Interferometer (IASI) is a high resolution Fourier Transform Spectrometer based on a Michelson Interferometer coupled to an integrated imaging system that measures infrared radiation emitted from the Earth. Developed by the Centre National d'Etudes Spatiales (CNES) in collaboration with the European Organisation for the Exploitation of Meteorological Satellites (EUMETSAT), IASI was launched in October 2006 onboard the polar-orbiting Meteorological Operational Platform (MetOp-A), and is operational since July 2007. IASI provides 8461 spectral

samples, ranging from 645 cm^{-1} to 2760 cm^{-1} (15.5 μm and 3.6 μm), with a spectral sampling of 0.25 cm^{-1}, and a spectral resolution of 0.5 cm^{-1} after apodisation ("Level 1c" spectra). IASI is an across track scanning system, whose swath width is of 2200 km, allowing global coverage twice a day. The IFOV is sampled by 2 × 2 circular pixels whose ground resolution is 12 km at nadir. In this study, use is made of the Level 1c data (available from the Ether Centre for Atmospheric Chemistry Products and Services website: http://ether.ipsl.jussieu.fr/, via EUMETCAST). Use is also made of the AMSU instruments flying onboard MetOp-A for cloud detection.

2.3 CARIBIC

CARIBIC (Civil Aircraft for the Regular Investigation of the Atmosphere Based on an Instrument Container) is a long-term scientific project conducting measurements of trace gases and aerosol particles in the upper troposphere and lowermost stratosphere (Brenninkmeijer et al., 2007). A comprehensive package of 18 individual instruments housed inside a 1.5 t air freight container is regulary loaded into a Lufthansa A340-600 passenger aircraft equipped with a specially designed air inlet. Measurement flights are performed over 2–4 consecutive days once per month during regular flights. Routine deployment of the current system started in May 2005 and is ongoing. The instrumentation includes an in-situ analyzer for continuous measurements of CO based on a commercial ultraviolet fluorescence instrument (Aero-Laser, AL 5002) which has been modified for use onboard aircraft (Scharffe et al., 2012). The instrument achieves a precision of 1–2 ppbv, the time resolution is 1 s. Calibration is in-flight every 25 min. Most measurements take place at cruise altitudes around 9–12 km, and data collected during ascent and descent were not used in this study.

2.4 The 4A fast line-by-line radiative transfer model

The radiative transfer simulations used in this study are performed by the 4A (Automatized Atmospheric Absorption Atlas) fast and accurate line-by-line radiative transfer

Title Page

Abstract | Introduction

Conclusions | References

Tables | Figures

◄ | ►►

◄ | ►

Back | Close

Full Screen / Esc

Printer-friendly Version

Interactive Discussion

T. Thonat et al.

model (Scott and Chédin, 1981; http://ara.abct.lmd.polytechnique.fr/). 4A is developed and maintained at the Laboratoire de Météorologie Dynamique. It has been made operational (OP) in cooperation with the French company Noveltis (see http://www.noveltis.net/4AOP/ for a description of 4AOP). 4A allows fast computation of the

5 transmittance of a discrete atmosphere along the vertical at a very high spectral resolution (5×10^{-4} cm^{-1} for this study) as well as the Jacobians (Chéruy et al., 1995) (with respect to temperature, mixing ratios and surface temperature and emissivity) for a user-defined observation level. It relies on comprehensive atlases of monochromatic optical thicknesses for up to 43 atmospheric molecular species. The atlases were

10 created by using the line-by-line and layer-by-layer model STRANSAC (Scott, 1974) in its latest version with up-to-date spectroscopy from the GEISA (Gestion et Etudes des Informations Spectroscopiques Atmosphériques, Management and Study of Spectroscopic Information) spectral line data catalog (Jacquinet-Husson et al., 2011). The 4AOP also includes up-to-date continua of N_2, O_2 and H_2O. It is the reference forward

15 radiative transfer model for the CNES/EUMETSAT IASI Level 1 Cal/Val activities and operational processing.

2.5 TIGR

The selection of AIRS and IASI channels presented in Sect. 3.1 is based on the TIGR (Thermodynamical Initial Guess Retrieval) atmospheric and radiative

20 database (Chédin et al., 1985; Chevallier et al., 1998) (available at http://ara.abct.lmd.polytechnique.fr/index.php?page=tigr). It comprises 2311 representative atmospheric situations selected by statistical method from 80 000 radiosonde reports. Each situation is described by its profiles of temperature, water vapour and ozone, a constant profile of CO, and constant profiles along the vertical of CO_2 (372 ppmv), N_2O (324 ppbv) and

25 CH_4 (1800 ppbv). From each atmospheric situation, 4A is used to compute the corresponding clear sky brightness temperatures, transmittances and Jacobians for the 2378 AIRS channels, the 8461 IASI channels and for all scan angles.

For all TIGR situations, the noise due to the instrument is computed using the following equation:

$$\mathrm{NE}\,\Delta T(\mathrm{BT}(v)) = \mathrm{NE}\,\Delta T\,(T_{\mathrm{ref}}(v))\,\frac{\frac{\partial B}{\partial T}(v, T_{\mathrm{ref}})}{\frac{\partial B}{\partial T}(v, \mathrm{BT}(v))} \tag{1}$$

where $\mathrm{NE}\,\Delta T$ is the equivalent noise temperature taken at the brightness temperature
5 BT, of the channel frequency v, and B is the radiance. For IASI, the reference noise corresponding to the reference temperature T_{ref} of 280 K is taken from the in-flight noise measurement (CNES, personal communication, 2009); for AIRS the reference noise at T_{ref} of 250 K was provided to us by the AIRS science team.

3   Study of infrared channels sensitivities

10 ### 3.1   Sensitivities of AIRS and IASI channels to atmospheric and surface perturbations

The 4.7 μm CO absorption band is located from about 2080 cm^{-1} to about 2200 cm^{-1}. Here we focus our analysis on the domain located from 2160 cm^{-1} (4.63 μm) to 2200 cm^{-1} (4.55 μm), where the strongest sensitivities to CO are found. Unlike IASI,
15 AIRS spectral domain does not cover completely the CO absorption band, since AIRS third spectral band begins at 2181.5 cm^{-1}.

In the 4.7 μm region, channels sensitive to CO are also sensitive to other variables that will be referred to as interferences (Crevoisier et al., 2003): surface temperature (T_s), surface emissivity (ε_s), temperature (T), water vapour (H_2O) and nitrous oxide
20 (N_2O). For each of the 872 TIGR tropical atmospheric situations, variations of brightness temperature induced by variations of atmospheric and surface vatiables are computed from the Jacobians:

$$\Delta BT(T) = \sum_{nl=1}^{nl=42} \frac{\partial BT}{\partial T}(nl) \times \Delta T(nl) \text{ for temperature} \tag{2}$$

$$\Delta BT\left(q_{gas}\right) = \sum_{nl=1}^{nl=42} \frac{\partial BT}{\partial q_{gas}}(nl) \times \Delta q_{gaz}(nl) \text{ for a gas} \tag{3}$$

where nl is the number of pressure layers.

The AIRS and IASI BT variations corresponding to variations of 1 K of temperature, 1 K of T_s, 10 % of CO, 20 % of H_2O, 2 % of N_2O, and 0.05 of surface emissivity (ε_s), are plotted in Fig. 1a and b.

The difference in spectral resolution between AIRS and IASI is well-seen in Fig. 1: $\sim 1.8\,\text{cm}^{-1}$ for AIRS at $2190\,\text{cm}^{-1}$ and $0.5\,\text{cm}^{-1}$ for IASI. This difference mostly explains the lower sensitivity of AIRS channels to CO. Moreover, AIRS only gives access to the end of the CO absorption band, which is characterized by lower intensities of the CO absorption lines. Channels located in the CO band are also strongly sensitive to T_s and to ε_s. Moreover, as the sensitivity to these two surface parameters gets weaker, the sensitivity to temperature and water vapour gets stronger. The sensitivity to N_2O is about 0.2 K for both AIRS and IASI at the end of the band. The radiometric noise, computed at the BT of the TIGR tropical scenes, is weaker for AIRS ($\sim 0.1\,\text{K}$) than for IASI ($\sim 0.2\,\text{K}$).

The comparison between the two instruments in terms of their suitability to measure CO in the atmosphere may be done by studying the ratio of the CO signal to the sum of the interferences signals, including the radiometric noise, hereafter referred to as the STI ratio (for Signal To Interferences ratio) (Crevoisier et al., 2003). Figure 1c shows that the STI ratio for IASI is about three times greater than for AIRS, which means that the weakness of the AIRS CO signal is not compensated by the weakness of the radiometric noise. High values of the STI ratios, for IASI and AIRS, are not only due to particularly low interferences, but also to relatively high sensitivities to CO, as seen in Fig. 1a and b.

Title Page

Abstract   Introduction

Conclusions   References

Tables   Figures

|◄   ►|

◄   ►

Back   Close

Full Screen / Esc

Printer-friendly Version

Interactive Discussion

3.2 Jacobians

The information about the distribution of the sensitivity along the vertical is given by the CO Jacobians. The averaged Jacobians computed with 4A on the TIGR tropical situations are plotted in Fig. 2 for the channels presenting the highest sensitivity to CO (see Fig. 1a and b). The shape of the Jacobians are similar for all these channels, with a maximum at about 450 hPa (~6.5 km), and half the maximum between about 750 (~2.5 km) and 200 hPa (~12 km), with the exception of the channel located at 2162.00 cm^{-1}, less sensitive to CO near the surface. The AIRS channels are sensitive to CO in the same part of the atmosphere, with a sensitivity almost three times weaker, in agreement with Fig. 1a and b.

As shown by Deeter et al. (2007) for MOPITT, the vertical sensitivity to CO varies especially near the surface with the thermal contrast, which is the difference between the surface temperature and the temperature of the first pressure level. Jacobians in Fig. 2a and b have been computed with no thermal contrast. Figure 2c and d shows the difference between these Jacobians and those computed with a +10 or −10 K thermal contrast. For both instruments, the higher the thermal contrast, the higher the sensitivity to CO in the lower part of the troposphere, particularly near the surface, with an opposite change of the sensitivity in the upper part of the troposphere. Negative and positive thermal contrasts have symmetric effects.

4 Retrieval method

4.1 Description of the method

The retrieval method is based on a double differential approach: a difference of channels and a difference between simulated and observed AIRS/IASI BT. The difference of channels is meant to be only sensitive to CO variations (see below); the corresponding simulations are computed with 4A, based on the description of the state of the

atmosphere given by the ECMWF reanalyses and an a priori CO profile. This double differential approach gives access to a signal only sensitive to CO in terms of BT. The corresponding CO mixing ratio (i.e. the difference with the a priori profile) is then computed by taking into account the sensitivity to CO of the selected channels given by the Jacobians. Overall, the retrieval process can be divided into 3 steps.

First, channels to be used in the retrieval process are selected. This selection is based on the study of the sensitivities of the channels (see Sect. 3). Couples of channels having the same sensitivities to every atmospheric and surface variable but CO are selected. The difference between the two channels of each couple is thus mostly sensitive to CO, and minimizes the sensitivity to the interferences. In order to lower the sensitivity to the atmospheric situation, the standard deviation of the differences has also to be minimum over the 872 TIGR tropical situations. Three couples of channels satisfying these criteria have been selected for each instrument. They are given in Tables 1 and 2 together with their characteristics and shown as crosses in Fig. 1. They are very weakly sensitive to N_2O, and almost not to O_3. The radiometric noise for these six channels ranges from 0.09 to 0.13 K for AIRS, with a standard deviation smaller than 0.03 K; for IASI it ranges from 0.19 to 0.23 K, with a standard deviation below 0.05 K.

Second, ECMWF (European Centre for Medium-Range Weather Forecasts) ERA-Interim Reanalyses (http://www.ecmwf.int/; Dee et al., 2011) profiles of T, H_2O and O_3 characterized by a 6 h time resolution and a $0.75° \times 0.75°$ space resolution, are colocalised both in time and space to every IASI or AIRS clear-sky FOV and inter/extrapolated on the 4A pressure levels. T_s is estimated directly from one IASI or AIRS channel in order to avoid the lag between the closest reanalyses and the IASI or AIRS passing. Use is made of the IASI BT at 2501.75 cm^{-1} and the AIRS BT at 2616.38 cm^{-1} (E. Péquignot, personal communication, 2012). Table 3 shows the characteristics of these two channels. They are characterized by a very high surface transmission. Based on comparisons between simulations and observations, T_s is equal to IASI/AIRS BT plus 2 K. Surface emissivity is fixed at 0.98. Based on the spectral

Title Page

Abstract | Introduction

Conclusions | References

Tables | Figures

|◄ | ►|

◄ | ►

Back | Close

Full Screen / Esc

Printer-friendly Version

Interactive Discussion

variations of ε_s retrieved from IASI (Capelle et al., 2012), ε_s does not vary much for the channels used in this study.

Third, T, H_2O and O_3 profiles, T_s and ε_s are used as inputs to 4A to simulate BT^{4A}, for each FOV and each channel. Then we calculate ΔBT as follows:

$$\Delta BT = \left(BT^{4A} - BT^{Sounder}\right)_{channel1} - \left(BT^{4A} - BT^{Sounder}\right)_{channel2} \qquad (4)$$

where channel 1 is the channel sensitive to CO and channel 2 the one which is not sensitive to it. ΔBT is a signal in K, which is thus only sensitive to the excess of CO in the troposphere compared to the 4A CO reference profile, referred to as ΔqCO. Using the sensitivities computed from the Jacobians (Eq. 3), we derive ΔqCO.

The retrieval method relies on the concurrent use of 4A model based simulations and observations. Therefore, potential systematic biases between simulations and observations must be removed. They are computed for each channel, by day and by night, by averaging, over the tropics (30° S, 30° N) and over the three first years of the operation of IASI (August 2007–July 2010) and over January–October 2008 for AIRS, the difference between simulations and collocated (in time and space) satellite observations. The simulations are performed using 4A with radiosonde measurements from the ARSA (Analyzed RadioSounding Archive) database (available at http://ara.lmd.polytechnique.fr/) as inputs. The radiative biases are added to BT^{4A} in Eq. (4).

4.2 Clouds and aerosols

Retrievals are performed in clear-sky only. To detect clouds and aerosols for AIRS data, use is made of several threshold tests based on AIRS and AMSU BT, allowing to discriminate low, medium and high clouds and aerosols (Crevoisier et al., 2003; Pierangelo et al., 2004). A similar method is applied to IASI and AMSU observations. Although efficient, the detection tests might not detect some observations weakly influenced by dust aerosols or by biomass burning aerosols which could particularly impact

Application to four years of Aqua/AIRS and MetOp-A/IASI

T. Thonat et al.

the retrievals since CO is emitted mostly by fires in the tropics. In the following, we evaluate the difference between BT in clear-sky conditions and BT with aerosols layers located at different altitudes simulated by 4A coupled to the DISORT model (Stamnes et al., 1988), based on the TIGR situations. Following Chédin et al. (2005), we assume

5 that biomass burning aerosol is a mixture of insoluble aerosol (INSO), water soluble aerosol (WASO) and black carbon aerosol (SOOT). Their optical properties are taken from the Optical Properties of Aerosol and Cloud database (Hess et al., 1998), and the infrared AOD is set to 0.05 at 10 µm. For the dust aerosol (or mineral transported aerosols, MITR), the AOD is set to 0.2. The results are shown in Tables 4 and 5.

10 The AIRS and IASI channels used to retrieve CO show a weak sensitivity to aerosols, especially to biomass burning aerosols. For both instruments, the maximum perturbation induced by smoke aerosols on BT reaches about 0.17 K, which is in the order of the 10 % CO signal for AIRS channels and smaller than the one for IASI channels. For dust aerosols the effect is more important, reaching about 0.80 K near 7 km altitude. How-

15 ever, the aerosols effect is cancelled by taking the difference between the two channels of each selected couple, since both channels of each couple have a similar sensitivity to the aerosols. Applying Eq. (3) to these simulated perturbations of BT, the impact of aerosols on the retrieved CO content is assessed. For smoke, it is less than 0.14 ppbv for AIRS, and less than 0.09 ppbv for IASI, which is negligible in both cases. The effect

20 of dust aerosols is more important, but still very weak: less than 0.81 ppbv for AIRS, and less than 0.46 ppbv for IASI.

4.3 Weighting functions

Our retrieval method gives access to an integrated content of CO in the low-to-mid troposphere. In order to derive a theoretical weighting function of CO, which indicates

25 the vertical sensitivity of the retrieval to a variation of CO, the method is first applied to the TIGR database. Both AIRS and IASI weighting functions are plotted in Fig. 3. As expected, they are very close to the CO Jacobians (Fig. 2), with a maximum of sensitivity around 450 hPa (∼6.5 km), and half a maximum between about 200 hPa

(~12 km) and about 750 hPa (~2.5 km). IASI and AIRS are sensitive to the same part of the troposphere, enabling a direct comparison of the CO column retrieved from both instruments.

The effect of the thermal contrast on the weighting functions is also shown in Fig. 3. The higher the thermal contrast, the higher the sensitivity to CO near the surface, and the lower the sensitivity in the mid troposphere. Compared to the weighting function with no thermal contrast, the maximum of the weighting function is lower by about 50 hPa (~0.8 km) for the +10 K thermal contrast, and higher by about 50 hPa (~0.8 km) for the −10 K case. Taking the difference of BT between two channels of a selected couple allows cancelling the effect of T_s on them. However, there is still a dependency on T_s via its effect on the sensitivity to CO of a given channel.

5 Results

The method is now applied to observations made by AIRS and IASI for the period July 2007–June 2011, over (30° S, 30° N), over land and over sea, by day and by night.

5.1 Assessing the precision of the method

The precision of the retrievals is evaluated by applying random variations to the input variables and then by computing the effects of such variations on the retrieved CO mixing ratio. For each situation (i.e. for each $0.75° \times 0.75°$ grid cell), T_s, profiles of T, H_2O and N_2O are randomly modified using a normal distribution with a 0 mean and standard deviations of 3 K, 2 K, 10 % and 2 % respectively.

Resulting induced variations of CO mixing ratios are computed for January and July 2008, for a random selection of 1 % of all situations over southern Africa. For both AIRS and IASI, the differences between the "modified CO" and the "reference CO" are on average less than 0.10 ppbv, with standard deviations of about 2.50 ppbv. The contribution of each variable to the total standard deviation is summarized in Table 6.

For IASI, the major influence on the CO retrievals comes from the temperature profile, with standard deviations of 1.64 and 2.00 ppbv for January and July respectively. The difference of the BT in each couple increases with T (as expected from Table 2). For AIRS, the influence of the temperature is lower than for IASI: the standard deviations are about 1.2 ppbv. This is explained by the fact that the variations of AIRS BT for each couple are of opposite signs and thus compensate one another (see Table 1). Moreover, for the region studied here, reanalyses are closer to AIRS passing than to IASI.

The results obtained when varying T_s highlights the strength of our differential method. Although the channels sensitivities to T_s are very important, its effect cancels out when making the BT difference: for IASI, the standard deviations are less than 0.9 ppbv. For AIRS, the contribution of T_s is bigger, and the standard deviations can reach 2 ppbv. This comes from the bigger sensitivity to T_s of the AIRS couples (see Table 1).

The influence of N_2O is more important for IASI than for AIRS, due to a lower sensitivity to N_2O of AIRS couples. The differences between the "modified CO" and the "reference CO" are on average quasi null with standard deviations of about 1.3 ppbv for IASI and about 0.3 ppbv for AIRS. N_2O slightly perturbs the BT of IASI channels, and, as shown in Table 1, the difference of sensitivities to N_2O has the same sign for each couple. Thus there is no compensation of the N_2O effect on CO between the three couples, which could induce a small systematic bias.

Last, the influence of water vapour on the CO retrievals is very weak for IASI, with quasi null average differences and standard deviations of less than 0.6 ppbv. The influence of water vapour on AIRS CO retrievals is more important. The average differences are almost null but standard deviations can reach 1.6 ppbv. The difference of sensitivities to H_2O has the same sign for each AIRS couple, so here there is no compensation between the couples.

Title Page

Abstract | Introduction

Conclusions | References

Tables | Figures

◄ | ►

◄ | ►

Back | Close

Full Screen / Esc

Printer-friendly Version

Interactive Discussion

5.2 Comparison with CARIBIC

AIRS and IASI CO retrievals are compared to CARIBIC CO measurements (Brenninkmeijer et al., 2007; Scharffe et al., 2012). While analyzing the results of this comparison, one has to keep in mind that CARIBIC measures CO at a given altitude in the range 9–12 km whereas an integrated content of tropospheric CO is retrieved from AIRS and IASI (see Sect. 4.3). Use is made of CARIBIC measurements from a total of 104 flights made over four different tropical regions from July 2007 to July 2011: China, India, Africa and the Caribbean. Six examples of flights and corresponding AIRS and IASI orbits are shown in Fig. 4. More FOVs are available for AIRS than for IASI (see Sect. 2) yielding somehow denser orbits. Over Africa, measurements are available between 30° N and 30° S. The three flights shown in Fig. 4a–c took place in October 2009 and November and December 2010, which are transition months between the fire seasons in the Southern Hemisphere (SH) and in the Northern Hemisphere (NH). A good agreement is seen between CARIBIC measurements and AIRS and IASI CO for all latitudes: low values are found for higher latitudes with CO increasing progressively while getting closer to the equator; a good agreement is also seen over the Saharian desert, which is a region characterised by a strong variability in emissivity. The same patterns are found with CARIBIC, AIRS and IASI: (i) in October, values above 110 ppbv are only found in SH, near 10° S, by CARIBIC, AIRS and IASI; (ii) in November, such values are found both in NH and SH, but with still higher values in SH; (iii) in December, they are mostly concentrated near the equator. For flight 321 (12 October 2010) CARIBIC measured very high values between 5° S and 5° N, reaching sometimes more than 200 ppbv, that are not seen by AIRS or IASI. This can be explained by the lack of CO retrievals near the equator due to the presence of clouds, and also by the fact that there is a time shift between the flights and the satellites passings which matters particularly near such time-dependant sources as fires. For flight 321, the aircraft passed about 3.5 h before and 8 h after the nearest two IASI orbits, and about 8 h before and 4 h after the nearest AIRS ones.

Over the Atlantic Ocean (Fig. 4d), comparison with flight 286 (23 September 2009) north-east of South America highlights that smaller variations than in Africa are seen along the flight by the sounders and CARIBIC. A steep increase occurs at the end of the flight near 12° S, where no AIRS or IASI retrievals are available; however, the latitudinal gradient seen along the flight track is well-seen by the sounders around 50° W. Finally, over India (Fig. 4e) for flight 228 (23 April 2008), and China (Fig. 4f) for flight 210 (24 October 2007), two montanuous regions, the evolution of CO along the flights is also quite well reproduced. Over China, one AIRS orbit exhibits particularly high CO values, reaching 140 ppbv, that are not seen by CARIBIC; the time lags between the sounder and the flight, that matter particularly in such a polutted area, might explain this discrepency.

More quantitatively, agreement between AIRS/IASI CO and CARIBIC CO is assessed by collocating in time and space CARIBIC and AIRS/IASI CO. For this, CARIBIC CO data are averaged over 1° along the flight track and colocalised with 1° × 1° average AIRS and IASI retrievals. For the comparisons, only aircraft measurements higher than 5 km altitude, to be far enough from the sources and close to the altitude seen by the sounders, with a time gap of less than five hours between the aircraft and AIRS or IASI, and grid cells with at least 5 AIRS or IASI FOVs are selected. Figure 5 shows CARIBIC CO against AIRS and IASI CO and the associated regression lines. The corresponding linear regression coefficients (R) are given in Table 7, together with the biases, standard deviations and relative differences between CARIBIC CO and the retrieved CO. The relative difference is defined as followed (e.g. Pommier et al., 2010):

$$\text{relative difference} = \frac{(\text{CARIBIC} - \text{Sounder}) \times 2}{(\text{CARIBIC} + \text{Sounder})}. \tag{5}$$

The difference between CARIBIC and AIRS is on average 6.1 ppbv, with a standard deviation of 18.4 ppbv and a relative difference of 4.92 %. The annual regression coefficient is 1.21. The agreement between CARIBIC and IASI is better, with a difference of

3.6 ppbv and a standard deviation of 13.0 ppbv. The relative difference is also smaller, reaching 3.42 %, as is the regression coefficient (1.08). Some differences are found between each season. For March-April-May (MAM), the standard deviation is higher than 20 ppbv for AIRS and IASI but the relative error is lower than the one for most of the other seasons, due to the high CO background. Indeed, differences above 40 ppbv are found over Africa and China where CARIBIC saw several extreme events that were not seen by AIRS and IASI. This is also the case in December-January-February (DJF). Especially over Southeast China such events are frequently encountered by the CARIBIC aircraft (Lai et al., 2011). In June-July-August (JJA), a smaller standard deviation is found corresponding to a higher relative error, due to low CO and an absence of strong emissions. The better agreement between CARIBIC and IASI can be attributed to the better suitability of IASI to retrieve CO, stemming from its spectral characteristics (see Sect. 3.1).

5.3 AIRS and IASI retrievals

Maps of monthly means of AIRS and IASI retrieved columns of CO are plotted in Fig. 6 for January, April, July and October 2008. White areas denote lack of observations due to persistent cloudiness. Some areas seen by IASI are not seen by AIRS due to too strong a cloud detection used for AIRS. The maps show a very good agreement between AIRS and IASI in terms of oceanic background values and spatial distribution over land. The extreme concentrations of CO located in northern Africa in January and April and in southern Africa in July and October are a consequence of strong biomass fires occurring there during the dry seasons. High concentrations west of these burning areas in the Atlantic and also South-East in October over the Indian Ocean highlight the transport pathways of fire emissions (Guan et al., 2008). In October, fire emissions are also seen over South America, with a small signal in the North in April and a much bigger one in Amazonia in October, with transported emissions over the Atlantic (Freitas et al., 2006). In Asia, high CO values are found in India and South-East Asia with fire emissions spreading in the Indian Ocean in January; in April emissions are stronger

in China and are transported over the Pacific Ocean. In July and October, relatively high CO values are still located over China, due to persistent pollution. Independently of these extreme values, there is a sharp south-north gradient of CO, explained by strongest continuous pollution sources located in the Northern Hemisphere.

The evolution of tropospheric CO over land from July 2007 to June 2011 is seen in Fig. 7 for the tropical regions. AIRS and IASI display the same evolution of CO during this period in terms of seasonality, seasonal amplitudes and year-to-year variability. CO is higher during winter, reaching a maximum at the end of the dry season, in March or April in NH, and in October in SH. The background level of CO is higher in the North, whereas the amplitude of the seasonal cycle is higher in the southern tropics due to stronger fire emissions. Consequently, the year-to-year variability is much lower in NH than in SH, where an increase in maximum CO values occurred in 2010, following a decrease after 2007 (see below). Figure 7 also shows the evolution of the GFEDv3 CO fire emissions (van der Werf et al., 2010) and the MODIS Burned Area (BA) (Roy et al., 2008) for the same period and the same area. In NH, the maximum of the BA and the emissions happens in December, with a secondary peak in March, whereas a little increase in CO is seen in December or January, and the maximum reached in March or April. In SH, fires are active between May and November, reaching a maximum of activity around August; according to AIRS and IASI, the maximum of CO in the troposphere is reached two months later.

The good match between these two fire products and CO concentrations confirms that the evolution of tropospheric CO in the tropics is mostly driven by fire activity (Duncan and Logan, 2008). The excess of CO in the troposphere seen by AIRS and IASI has the same duration as the fire season, but with a shift of about two months. This has already been observed for southern Africa (van der Werf et al., 2006; Roberts et al., 2009), where it might be explained by the predominance of woodland burning at the end of the dry season. Moreover, CO is emitted mostly in the smoldering phase of the combustion (Lobert and Warnatz, 1993), which implies conditions of higher moisture and lower temperature found at the end of the dry season.

Application to four years of Aqua/AIRS and MetOp-A/IASI

T. Thonat et al.

Title Page

Abstract | Introduction

Conclusions | References

Tables | Figures

◄◄ | ►►

◄ | ►

Back | Close

Full Screen / Esc

Printer-friendly Version

Interactive Discussion

Figure 8 shows the evolution of CO and fire activity, respectively, for five tropical areas where strong biomass burning takes place every year. In South America (Fig. 8a and b) the excess of CO is observed between August and November; according to the two fire products, the fire season occurs between June and October. A secondary

5 CO peak is seen between February and April, caused by the smaller fire activity in January in the northern part of the area. South America has experienced a strong year-to-year variability in terms of CO, that can be explained by the variability in fires, in relation with climate conditions. Figure 9 displays the Southern Oscillation Index (SOI), the Multivariate ENSO Index and the Atlantic Multidecadal Oscillation (AMO).

10 The decrease in maximum CO values from 2007 to 2009 is in good agreement with the decreasing activity of fires during the same period, which was characterized by average climate conditions, as seen in Fig. 9. On the contrary, in 2010, the very high AMO coupled to the remaining El Niño conditions in the beginning of 2010 (Fig. 9) induced a severe drought in Amazonia (Lewis et al., 2011), which explains the increase

15 in fire activity and, subsequently, the increase in CO concentrations.

In North Africa (Fig. 8c and d), CO is higher between November and March while the fire season occurs between October and February. The excess of CO is still important until August, which might be caused by the transport of fire emissions from southern Africa. The seasonality of CO in South Africa (Fig. 8e and f) can be more directly

20 related to fire activity. The excess of CO is observed between July and December, with remaining high values between January and March, revealing the impact of transported emissions from northern Africa fire emissions. As observed in South America, there is a sharp increase in CO in 2010 compared to previous years, which can be explained by the increase in the burned area observed this year in relation with ENSO (Fig. 9).

25 In South-East Asia (Fig. 8g and h), CO displays two maxima per year, the first one between March and May, the other one around October–November. The minimum in this region occurs around July–August. GFEDv3 shows two peaks in the emissions in 2009, in March and September, which can explain the evolution of CO this year. However, the high fire activity seen in March 2010 with the two fire products does not

seem to have entailed a significant change in CO evolution. The discrepancies between the BA and GFEDv3 suggest that fires behaviour is somehow difficult to assess in this area.

Finally, in Australia (Fig. 8i and j), excess of CO occurs between August and December, with a maximum in October, which matches quite well fire activity. The increase in CO begins in May, which is again consistent with fire activity. As well as for South America and South Africa, there is a decrease in maximum CO values after 2007 and an increase of the maximum in October 2010. However, for Australia, this interannual variability does not seem to be directly supported by the variability of fires.

Figure 10 shows the monthly evolution of IASI CO for 12 latitudinal bands of 5° each, over the Western Pacific between Australia and Japan, an area where aircraft measurements of CO were routinely performed between 1993 and 2001 (Matsueda et al., 1999). Matsueda et al. (2002) have shown that CO seasonality in this region was dependent on Indonesian fires and closely related to the ENSO events. Figure 10 shows the latitudinal variations of CO, and can be directly compared to Fig. 1 of Matsueda et al. (2002). A very good agreement in the seasonality is seen at all latitudes when comparing both figures. The highest seasonal amplitude of CO is found near 25° N and S, but the background level is higher in the North, reaching 80 ppbv for (25° N, 30° N) whereas it is about 50 ppbv for (30° S, 25° S). In the Northern Hemisphere, CO is maximum in April while it is minimum in the South; the maximum in the South occurs in October–November while it reaches a minimum in the North. Figure 10 also shows an increase in maximum CO values in 2010, at the beginning of the year in NH. Early 2010 shows El Niño conditions that may have caused the large increase in fire emissions seen from GFEDv3 in Fig. 8h. There is also an increase at the end of the year in SH although MODIS BA and GFEDv3 do not report significant increase in fire activity.

6   Conclusions

Four years (July 2007–June 2011) of tropospheric CO columns have been retrieved from AIRS and IASI observations in the tropics (30°S, 30° N). The retrieval method is based on a double differential approach: differences between channels which have the same sensitivities to every atmospheric and surface variable but CO; differences between observations and simulations, using the 4A radiative transfer model and the ECMWF reanalyses. The sensitivity to surface temperature (T_s) cancels out when taking the BT differences which limits its influence on the retrieved CO signal; however T_s still influences the part of the atmosphere seen by the sounders. The sensitivity to CO along the vertical depends on the thermal contrast (i.e. the difference between the surface temperature and the temperature of the first pressure level): the higher the thermal contrast the higher the sensitivity to CO near the surface. Weighting functions associated to the mid-troposphere integrated content of CO retrieved from IR channels display a maximum of sensitivity around 450 hPa (∼6.5 km), with half the maximum between 200 hPa (∼12 km) and 750 hPa (∼2.5 km). The effects of aerosols have also been assessed on CO retrieval using simulations based on the 4A/DISORT model. For both smoke and dust aerosols, their impact almost cancels out when taking the BT differences, the resulting effect on the CO retrievals being for less than 1 ppbv. The retrieval process has been shown to be weakly sensitive to the atmospheric and surface input data, with an associate bias in CO less than 0.10 ppbv and a standard deviation less than 3 ppbv.

AIRS and IASI retrievals have been compared to CARIBIC aircraft measurements. Relative differences are found to be 4.92 % and 3.42 % for AIRS and IASI respectively, with coefficients in linear regression of CARIBIC on the sounders of 1.21 and 1.08. The better agreement between CARIBIC and IASI comes from its better spectral resolution, which helps discriminating CO from other signals, and the coverage of the full CO absorption band (which yields channels characterized by stronger sensitivity to CO). The twice better noise of AIRS compared to IASI does not compensate for this difference

in terms of spectral resolution (1.8 vs. $0.5\,\mathrm{cm}^{-1}$). This indicates that an improvement of both spectral and radiometric characteristics should be a priority for future instruments. Further comparisons with other CO retrievals from TIR sounders will be performed in the future. As stressed for example by George et al. (2009), these comparisons require
5 to take into account the differences between the retrievals in the a priori and the vertical sensitivities, which would constitute a study on its own.

   AIRS and IASI CO show a very good agreement in terms of seasonality, seasonal amplitudes, interannual variability and spatial distribution, as well as in terms of absolute value. The CO evolution in the tropics is mostly driven by fire emissions. In the
10 northern tropics, where the background level of CO is higher than in the southern tropics, there have not been any important internannual variations in CO because no major changes took place over the 4 yr period studied here. On the contrary, the southern tropics, where stronger fire events take place, display a strong interannual variability, with a sharp decrease after 2007 followed by a large increase in 2010 in relation with
15 El Niño conditions in early 2010 and the exceptionally high AMO throughout 2010.

   Using both AIRS and IASI, whose Equator crossing-times are respectively 01:30 and 09:30 a.m./p.m. LT, gives access to four CO retrievals a day highlighting the great possibility of studying the diurnal cycle of CO from infrared sounders onboard polar satellites. Moreover, infrared sounders also enable to retrieve several gases emitted by fires,
20 either CO_2 or reactive trace species (Crevoisier et al., 2009; Coheur et al., 2009), giving the opportunity to study the correlations between all these gases from a single instrument. This possibility will be assured in the future with observations from the Fourier transform spectrometer CrIS (Cross-track Infrared Sounder) launched onboard the NPP (National Polar-orbiting Partnership) satellite in October 2011, and with the
25 launches of MetOp-B in May 2012 and MetOp-C in 2016, providing us with more than 20 yr of IASI observations.

The publication of this article is financed by CNRS-INSU.

AMTD

5, 3861–3908, 2012

Application to four years of Aqua/AIRS and MetOp-A/IASI

T. Thonat et al.

Title Page

Abstract	Introduction
Conclusions	References
Tables	Figures

|◄   ►|

◄   ►

Back   Close

Full Screen / Esc

Printer-friendly Version

Interactive Discussion

References

Brenninkmeijer, C. A. M., Crutzen, P., Boumard, F., Dauer, T., Dix, B., Ebinghaus, R., Filippi, D., Fischer, H., Franke, H., Frieß, U., Heintzenberg, J., Helleis, F., Hermann, M., Kock, H. H., Koeppel, C., Lelieveld, J., Leuenberger, M., Martinsson, B. G., Miemczyk, S., Moret, H. P., Nguyen, H. N., Nyfeler, P., Oram, D., O'Sullivan, D., Penkett, S., Platt, U., Pupek, M., Ramonet, M., Randa, B., Reichelt, M., Rhee, T. S., Rohwer, J., Rosenfeld, K., Scharffe, D., Schlager, H., Schumann, U., Slemr, F., Sprung, D., Stock, P., Thaler, R., Valentino, F., van Velthoven, P., Waibel, A., Wandel, A., Waschitschek, K., Wiedensohler, A., Xueref-Remy, I., Zahn, A., Zech, U., and Ziereis, H.: Civil Aircraft for the regular investigation of the atmosphere based on an instrumented container: The new CARIBIC system, Atmos. Chem. Phys., 7, 4953–4976, doi:10.5194/acp-7-4953-2007, 2007.

Buchwitz, M., de Beek, R., Bramstedt, K., Noël, S., Bovensmann, H., and Burrows, J. P.: Global carbon monoxide as retrieved from SCIAMACHY by WFM-DOAS, Atmos. Chem. Phys., 4, 1945–1960, doi:10.5194/acp-4-1945-2004, 2004.

Capelle, V., Chédin, A., Péquignot, E., Schluessel, P., Newman, S. M., and Scott, N. A.: Infrared continental surface emissivity spectra and skin temperature retrieved from IASI observations over the tropics, J. Appl. Meteorol. Clim., doi:10.1175/JAMC-D-11-0145.1, accepted, 2012.

Chédin, A., Scott, N. A., Wahiche, C., and Moulinier, P.: The improved initialization inversion method: a high resolution physical method for temperature retrievals from satellites of the TIROS-N series, J. Clim. Appl. Meteorol., 24, 128-143, 1985.

Chédin, A., Serrar, S., Scott, N. A., Pierangelo, C., and Ciais, P.: Impact of tropical biomass burning emission on the diurnal cycle of upper tropospheric CO_2 retrieved from NOAA 10 satellite observations, J. Geophys. Res., 110, D11309, doi:10.1029/2004JD005540, 2005.

Chéruy, F., Scott, N. A., Armante, R., Tournier, B., and Chédin, A.: Contribution to the development of radiative transfer models for high spectral resolution observations in the infrared, J. Quant. Spectrosc. Ra., 53, 597–611, 1995.

Chevallier, F., Chéruy, F., Scott, N. A., and Chédin, A.: A neural network approach for a fast and accurate computation of longwave radiative budget, J. Appl. Meteorol., 37, 1385–1397, 1998.

Title Page

Abstract | Introduction

Conclusions | References

Tables | Figures

|◄ | ►|

◄ | ►

Back | Close

Full Screen / Esc

Printer-friendly Version

Interactive Discussion

Clerbaux, C., Hadji-Lazaro, J., Payan, S., Camy-Peyret, C., and Mégie, G.: Retrieval of CO Columns from IMG/ADEOS Spectra, IEEE T. Geosci. Remote, 37, 1657–1661, 1999.

Coheur, P.-F., Clarisse, L., Turquety, S., Hurtmans, D., and Clerbaux, C.: IASI measurements of reactive trace species in biomass burning plumes, Atmos. Chem. Phys., 9, 5655–5667, doi:10.5194/acp-9-5655-2009, 2009.

Crevoisier, C., Chédin, A., and Scott, N. A.: AIRS channel selection for CO_2 and other trace-gas retrievals, Q. J. Roy. Meteorol. Soc., 129, 2719–2740, 2003.

Crevoisier, C., Chédin, A., Matsueda, H., Machida, T., Armante, R., and Scott, N. A.: First year of upper tropospheric integrated content of CO_2 from IASI hyperspectral infrared observations, Atmos. Chem. Phys., 9, 4797–4810, doi:10.5194/acp-9-4797-2009, 2009.

de Laat, A. T. J., Gloudemans, A. M. S., Schrijver, H., van den Broek, M. M. P., Meirink, J. F., Aben, I., and Krol, M.: Quantitative analysis of SCIAMACHY carbon monoxide total column measurements, Geophys. Res. Lett., 33, L07808, doi.1029/2005GL025530, 2006.

Dee, D. P., Uppala, S. M., Simmons, A. J., Berrisford, P., Poli, P., Kobayashi, S., Andrea, U., Balmaseda, M. A., Balsamo, G., Bauer, P., Bechtold, P., Beljaars, A. C. M., van de Berg, L., Bidlot, J., Bormann, N., Delsol, C., Dragani, R., Fuentes, M., Geer, A. J., Haimberger, L., Healy, S. B., Hersbach, H., Hólm, E. V., Isaksen, L., Kållberg, P., Köhler, M., Matricardi, M., McNally, A. P., Monge-Sanz, B. M., Morcrette, J.-J., Park, B.-K., Peubey, C., de Rosnay, P., Tavolato, C., Thépaut, J.-N., and Vitart, F.: The ERA-Interim reanalysis: configuration and performance of the data assimilation system, Q. J. Roy. Meteorol. Soc., 137, 553–597, doi:10.1002/qj.828, 2011.

Deeter, M. N., Emmons, L. K., Francis, G. L., Edwards, D. P., Gille, J. C., Warner, J. X., Khattatov, B., Ziskin, D., Lamarque, J.-F., Ho, S.-P., Yudin, V., Attié, J.-L., Packman, D., Chen, J., Mao, D., and Drummond, J. R.: Operational carbon monoxide retrieval algorithm and selected results for MOPITT instrument, J. Geophys. Res., 108, ACH1-1–ACH-1-11, doi:10.1029/2002JD003186, 2003.

Deeter, M. N., Edwards, D. P., Gille, J. C., and Drummond, J. R.: Sensitivity of MOPITT observations to carbon monoxide in the mower troposphere, J. Geophys. Res., 112, D24306, doi:10.1029/2007JD008929, 2007.

Deeter, M. N., Edwards, D. P., Gille, J. C., and Drummond, J. R.: CO retrievals based on MOPITT near-infrared observations, J. Geophys. Res., 114, D04303, doi:10.1029/2008JD010872, 2009.

Duncan, B. N. and Logan, J. A.: Model analysis of the factors regulating the trends and variability of carbon monoxide between 1988 and 1997, Atmos. Chem. Phys., 8, 7389–7403, doi:10.5194/acp-8-7389-2008, 2008.

Duncan, B. N., Logan, J. A., Bey, I., Megretskaia, I. A., Yantosca, R. M., Novelli, P. C., Jones, N. B., and Rinsland, C. P.: Global budget of CO, 1988–1997: Source estimates and validation with a global model, J. Geophys. Res., 112, D22301, doi:1029/2007JD008459, 2007.

Edwards, D. P., Emmons, L. K., Hauglustaine, D. A., Chu, D. A., Gille, J. C., Kaufman, Y. J., Pétron, G., Yurganov, L. N., Giglio, L., Deeter, M. N., Yudin, V., Ziskin, D. C., Warner, J., Lamarque, J.-F., Francis, G. L., Ho, S. P., Mao, D., Chen, J., Grechko, E. I., and Drummond, J. R.: Observations of carbon monoxide and aerosols from Terra satellite: Northern Hemisphere variability, J. Geophys. Res., 109, D24202, doi:10.1029/2004JD004727, 2004.

Fortems-Cheney, A., Chevallier, F., Pison, I., Bousquet, P., Szopa, S., Deeter, M. N., and Clerbaux, C.: Ten years of CO emissions as seen from Measurements of Pollution in the Troposphere (MOPITT), J. Geophys. Res., 116, D05304, doi:10.1029/2010JD014416, 2011.

Frankenberg, C., Platt, U., and Wagner, T.: Retrieval of CO from SCIAMACHY onboard ENVISAT: detection of strongly polluted areas and seasonal patterns in global CO abundances, Atmos. Chem. Phys., 5, 1639–1644, doi:10.5194/acp-5-1639-2005, 2005.

Freitas, S. R., Longo, K. M., and Andreae, M. O.: Impact if including the plume rise of vegetation fires in numerical simulations of associated atmospheric pollutants, Geophys. Res. Lett., 33, L17808, doi:10.1029/2006GL026608, 2006.

George, M., Clerbaux, C., Hurtmans, D., Turquety, S., Coheur, P.-F., Pommier, M., Hadji-Lazaro, J., Edwards, D. P., Worden, H., Luo, M., Rinsland, C., and McMillan, W.: Carbon monoxide distributions from the IASI/METOP mission: evaluation with other space-borne remote sensors, Atmos. Chem. Phys., 9, 8317–8330, doi:10.5194/acp-9-8317-2009, 2009.

Guan, H., Chatfield, R. B., Freitas, S. R., Bergstrom, R. W., and Longo, K. M.: Modeling the effect of plume-rise on the transport of carbon monoxide over Africa with NCAR CAM, Atmos. Chem. Phys., 8, 6801–6812, doi:10.5194/acp-8-6801-2008, 2008.

Hess, M., Koepke, P., and Schult, I.: Optical Properties of Aerosols and Clouds: The software package OPAC, B. Am. Meteorol. Soc., 79, 831–844, 1998.

Hilton, F., Armante, R., August, T., Barnet, C., Bouchard, A., Camy-Peyret, C., Capelle, V., Clarisse, L., Clerbaux, C., Coheur, P.-F., Collard, A., Crevoisier, C., Dufour, G., Edwards, D., Faijan, F., Fourrié, N., Gambacorta, A., Goldberg, M., Guidard, V., Hurtmans, D., Illingworth, S., Jacquinet-Husson, N., Kerzenmacher, T., Klaes, D., Lavanant, L., Masiello, G., Matricardi,

Title Page

Abstract | Introduction

Conclusions | References

Tables | Figures

|◄ | ►|

◄ | ►

Back | Close

Full Screen / Esc

Printer-friendly Version

Interactive Discussion

M., McNally, A., Newman, S., Pavelin, E., Payan, S., Péquignot, E., Peyridieu, S., Phulpin, T., Remedios, J., Schlüussel, P., Serio, C., Strow, L., Stubenrauch, C., Taylor, J., Tobin, D., Wolf, W., and Zhou, D., Hyperspectral Earth Observation from IASI: Five Years of Accomplishments, B. Am. Meteorol. Soc., 93, 347–370, doi:10.1175/BAMS-D-11-00027.1, 2012.

Holloway, T., Levy II, H., and Kasibhatla, P.: Global distribution of carbon monoxide, J. Geophys. Res., 105, 12123–12147, 2000.

Illingworth, S. M., Remedios, J. J., Boesch, H., Moore, D. P., Sembhi, H., Dudhia, A., and Walker, J. C.: ULIRS, an optimal estimation retrieval scheme for carbon monoxide using IASI spectral radiances: sensitivity analysis, error budget and simulations, Atmos. Meas. Tech., 4, 269–288, doi:10.5194/amt-4-269-2011, 2011.

Jacquinet-Husson, N., Crepeau, L., Armante, R., Boutammine, C., Chédin, A., Scott, N. A., Crevoisier, C., Capelle, V., Boone, C., Poulet-Crovisier, N., Barbe, A., Campargue, A., Benner, C. D., Benilan, Y., Bézard, B., Boudon, V., Brown, L. R., Coudert, L. H., Coustenis, A., Dana, V., Devi, V. M., Fally, S., Fayt, A., Flaud, J.-M., Goldman, A., Herman, M., Harrio, G. J., Jacquemart, D., Jolly, A., Kleiner, I., Kleinböhl, A., Kwabia-Tchana, F., Lavrentieva, N., Lacome, N., Li-Hong, X., Lyulin, O. M., Mandin, J.-Y., Maki, A., Mikhailenko, S., Miller, C. E., Mishina, T., Moazzen-Ahmadi, N., Müller, H. S. P., Nikitin, A., Orphal, J., Perevalov, V., Perrin, A., Petkie, D. T., Predoi-Cross, A., Rinsland, C. P., Remedios, J. J., Rotger, M., Smith, M. A. H., Sung, K., Tashkun, S., Tennyson, J., Toth, R. A., Vandaele, A.-C., and Vander Auwera, J.: The 2009 edition of the GEISA spectroscopic database, J. Quant. Spectrosc. Ra., 112, 2395–2445, doi:10.1016/j.jqsrt.2011.06.004, 2011.

Kopacz, M., Jacob, D. J., Fisher, J. A., Logan, J. A., Zhang, L., Megretskaia, I. A., Yantosca, R. M., Singh, K., Henze, D. K., Burrows, J. P., Buchwitz, M., Khlystova, I., McMillan, W. W., Gille, J. C., Edwards, D. P., Eldering, A., Thouret, V., and Nedelec, P.: Global estimates of CO sources with high resolution by adjoint inversion of multiple satellite datasets (MOPITT, AIRS, SCIAMACHY, TES), Atmos. Chem. Phys., 10, 855–876, doi:10.5194/acp-10-855-2010, 2010.

Lai, S. C., Baker, A. K., Schuck, T. J., Slemr, F., Brenninkmeijer, C. A. M., van Velthoven, P., Oram, D. E., Zahn, A., and Ziereis, H.: Characterization and source regions of 51 high-CO events observed during Civil Aircraft for the Regular Investigation of the Atmosphere Based on an Instrument Container (CARIBIC) flights between south China and the Philippines 2005–2008, J. Geophys. Res., 116, D20308, doi:10.1029/2011JD016375, 2011.

Application to four years of Aqua/AIRS and MetOp-A/IASI

T. Thonat et al.

Title Page

Abstract | Introduction

Conclusions | References

Tables | Figures

◄ | ►

◄ | ►

Back | Close

Full Screen / Esc

Printer-friendly Version

Interactive Discussion

Lewis, S. L., Brando, P. M., Phillips, O. L., van der Heijden, G. M. F., and Nepstad, D.: The 2010 Amazon drought, Science, 331, p. 554, 2011.

Lobert, J. M. and Warnatz, J.: Emissions from the combustion process in vegetation, in: Fire in the environment: The ecological, atmospheric, and climatic importance of vegetation fires, edited by: Crutzen, P. J. and Goldammer, J. G., Wiley, Chichester, 15–37, 1993.

Machida, T. Matsueda, H., Sawa, Y., Nakagawa, Y., Hirotani, K., Kondo, N., Goto, K., Nakazawa, T., Ishikawa, K., and Ogawa, T.: Worldwide measurements of atmospheric CO_2 and other trace gas species using commercial airlines. J. Atmos. Ocean. Tech., 25, 1744–1754, doi:10.1175/2008JTECHA1082.1, 2008.

Matsueda, H., Inoue, H. Y., Ishii, M., and Tsutsumi, Y.: Large injection of carbon monoxide into the upper troposphere due to intense biomass burning in 1997, J. Geophys. Res., 104, 26867–26879, 1999.

Matsueda, H., Taguchi, S., Inoue, H. Y., and Ishii, M.: A large impact of tropical biomass burning on CO and CO_2 in the upper troposphere, Sci. China, 45, 116-125, 2002.

McMillan, W. W., Barnet, C., Strow, L., Chahine, M. T., McCourt, M. L., Warner, J. X., Novelli, P. C., Korontzi, S., Maddy, E. S., and Datta, S.: Daily global maps of carbon monoxide from NASA's Atmospheric Infrared Sounder, Geophys. Res. Lett., 32, L11801, doi:10.1029/2004GL021821, 2005.

Nedelec, P., Cammas, J.-P., Thouret, V., Athier, G., Cousin, J.-M., Legrand, C., Abonnel, C., Lecoeur, F., Cayez, G., and Marizy, C.: An improved infrared carbon monoxide analyser for routine measurements aboard commercial Airbus aircraft: technical validation and first scientific results of the MOZAIC III programme, Atmos. Chem. Phys., 3, 1551–1564, doi:10.5194/acp-3-1551-2003, 2003.

Pierangelo, C., Chédin, A., Heilliette, S., Jacquinet-Husson, N., and Armante, R.: Dust altitude and infrared optical depth from AIRS, Atmos. Chem. Phys., 4, 1813–1822, doi:10.5194/acp-4-1813-2004, 2004.

Pommier, M., Law, K. S., Clerbaux, C., Turquety, S., Hurtmans, D., Hadji-Lazaro, J., Coheur, P.-F., Schlager, H., Ancellet, G., Paris, J.-D., Nédélec, P., Diskin, G. S., Podolske, J. R., Holloway, J. S., and Bernath, P.: IASI carbon monoxide validation over the Arctic during POLARCAT spring and summer campaigns, Atmos. Chem. Phys., 10, 10655–10678, doi:10.5194/acp-10-10655-2010, 2010.

Reichle Jr., H. G., Anderson, B. E., Connors, V. S., Denkins, T. C., Forbes, D. A., Gormsen, B. B., Lagenfelds, R. L., Neil, D. O., Nolf, S. R., Novelli, P. C., Pougatchev, N. S., Roell, M. M., and Steele, L. P.: Space shuttle based global CO measurments during April and October 1994, MAPS instrument, data reduction, and data validation, J. Geophys. Res., 104, 21443–21454, 1999.

Rinsland, C. P., Luo, M., Logan, J. A., Beer, R., Worden, H., Rider, D., Osterman, G., Gunson, M., Eldering, A., Goldman, A., Shephard, M., Cough, S. A., Rodgers, C., Lamperl, M., and Chiou, L.: Nadir measurements of carbon monoxide distributions by Tropospheric Emission Spectrometer instrument onboard the Aura Spacecraft: Overview of analysis approach and examples of initial results, Geophys. Res. Lett., 33, L22806, doi:10.1029/2006GL027000, 2006.

Rinsland, C. P., Luo, M., Shephard, M., Clerbaux, C., Boone, C. D., Bernath, P. F., Chiou, L., and Coheur, P. F.: Tropospheric emission spectrometer (TES) and atmospheric chemistry experiment (ACE) measurements of tropospheric chemistry in tropical southeast Asia during a moderate El Nino in 2006, J. Quant. Spectrosc. Ra., 109, 1931–1942, doi:10.1016/j.jqsrt.2007.12.020, 2008.

Roberts, G., Wooster, M. J., and Lagoudakis, E.: Annual and diurnal african biomass burning temporal dynamics, Biogeosciences, 6, 849–866, doi:10.5194/bg-6-849-2009, 2009.

Roy, D. P., Boschetti, L., Justice, C. O., and Ju, J.: The collection 5 MODIS burnt area product – Global evaluation by comparison with the MODIS active fire product, Remote Sens. Environ., 112, 3690–3707, 2008.

Scharffe, D., Slemr, F., Brenninkmejer, C. A. M., and Zahn, A.: Carbon monoxide measurements onboard the CARIBIC passenger aircraft using UV resonance fluorescence, Atmos. Meas. Tech. Discuss., 5, 2681–2702, doi:10.5194/amtd-5-2681-2012, 2012.

Scott, N. A.: A direct method of computation of the transmission function of an inhomogeneous gaseous medium – I: Description of the method, J. Quant. Spectrosc. Ra., 14, 691–704, doi:10.1016/0022-4073(74)90116-2, 1974.

Scott, N. A. and Chédin, A.: A fast line-by-line method for atmospheric absorption computations: The Automatized Atmospheric Absorption Atlas, J. Appl. Meteorol., 20, 556–564, 1981.

Stamnes, K., Tsay, S.-C., Wiscombe, W., and Jayaweera, K.,: Numerically sable algorithm for discrete ordinate-method radiative transfer in multiple scattering and emitting layered media, Appl. Optics, 27, 2502–2509, 1988.

Turquety, S., Clerbaux, C., Law, K., Coheur, P.-F., Cozic, A., Szopa, S., Hauglustaine, D. A., Hadji-Lazaro, J., Gloudemans, A. M. S., Schrijver, H., Boone, C. D., Bernath, P. F., and Edwards, D. P.: CO emission and export from Asia: an analysis combining complementary satellite measurements (MOPITT, SCIAMACHY and ACE-FTS) with global modeling, Atmos. Chem. Phys., 8, 5187–5204, doi:10.5194/acp-8-5187-2008, 2008.

Turquety, S., Hurtmans, D., Hadji-Lazaro, J., Coheur, P.-F., Clerbaux, C., Josset, D., and Tsamalis, C.: Tracking the emission and transport of pollution from wildfires using the IASI CO retrievals: analysis of the summer 2007 Greek fires, Atmos. Chem. Phys., 9, 4897–4913, doi:10.5194/acp-9-4897-2009, 2009.

van der Werf, G. R., Randerson, J. T., Giglio, L., Collatz, G. J., Kasibhatla, P. S., and Arellano Jr., A. F.: Interannual variability in global biomass burning emissions from 1997 to 2004, Atmos. Chem. Phys., 6, 3423–3441, doi:10.5194/acp-6-3423-2006, 2006.

van der Werf, G. R., Randerson, J. T., Giglio, L., Collatz, G. J., Mu, M., Kasibhatla, P. S., Morton, D. C., DeFries, R. S., Jin, Y., and van Leeuwen, T. T.: Global fire emissions and the contribution of deforestation, savanna, forest, agricultural, and peat fires (1997–2009), Atmos. Chem. Phys., 10, 11707–11735, doi:10.5194/acp-10-11707-2010, 2010.

WMO: Technical Report of Global Analysis Method for Major Greenhouse Gases by the World Data Center for Greenhouse Gases, GAW Report No. 184, WMO/TD – No. 1473, 2009.

Yurganov, N. L., McMillan, W. W., Dzhola, A. V., Grechko, E. I., Jones, N. B., and van der Werf, G. R.: Global AIRS and MOPITT CO measurements: Validation, comparison, and links to biomass burning variations and carbon cycle, J. Geophys. Res., 113, D09301, doi:10.1029/2007JD009229, 2008.

Application to four years of Aqua/AIRS and MetOp-A/IASI

T. Thonat et al.

Title Page

Abstract | Introduction

Conclusions | References

Tables | Figures

◄ | ►

◄ | ►

Back | Close

Full Screen / Esc

Printer-friendly Version

Interactive Discussion

Table 1. Sensitivities of AIRS selected channels, computed with 4A and averaged over the 872 TIGR tropical atmospheric situations.

AIRS Channels	Wave nb (cm^{-1})	CO 10 %	T_s 1 K	T 1 K	ε_s 0.05	H$_2$O 20 %	N$_2$O 2 %	O$_3$ 20 %
1867	2183.31	0.15	0.51	0.38	0.38	0.08	0.12	0.01
1876	2191.45	0.01	0.50	0.41	0.37	0.11	0.13	0.01
Difference		0.14	0.01	−0.03	0.01	−0.03	−0.01	0.01
Std of the difference		0.02	0.00	0.01	0.01	0.02	0.00	0.00
1874	2189.67	0.13	0.43	0.45	0.29	0.11	0.15	0.01
1873	2188.76	0.02	0.46	0.42	0.32	0.11	0.16	0.01
Difference		0.11	−0.03	0.03	−0.03	0.00	−0.01	0.00
Std of the difference		0.02	0.00	0.00	0.01	0.01	0.00	0.00
1874	2189.67	0.13	0.43	0.45	0.29	0.11	0.15	0.01
1877	2180.50	0.03	0.45	0.45	0.31	0.15	0.13	0.01
Difference		0.10	−0.03	0.00	−0.02	−0.04	0.01	0.00
Std of the difference		0.02	0.01	0.01	0.01	0.03	0.00	0.00

Title Page

Abstract | Introduction

Conclusions | References

Tables | Figures

|◀ | ▶|

◀ | ▶

Back | Close

Full Screen / Esc

Printer-friendly Version

Interactive Discussion

Table 2. Same as Table 1 for IASI.

IASI Channels	Wave nb (cm^{-1})	CO 10 %	T_s 1 K	T 1 K	ε_s 0.05	H$_2$O 20 %	N$_2$O 2 %	O$_3$ 20 %
6084	2165.75	0.40	0.64	0.33	0.57	0.10	0.01	0.01
6129	2177.00	0.03	0.64	0.25	0.54	0.07	0.10	0.02
Difference		0.37	0.00	0.08	0.03	0.03	−0.09	−0.01
Std of the difference		0.06	0.01	0.02	0.03	0.04	0.02	0.00
6126	2176.25	0.45	0.53	0.39	0.41	0.06	0.06	0.01
6138	2179.25	0.07	0.53	0.35	0.38	0.16	0.10	0.02
Difference		0.38	0.00	0.04	0.03	−0.10	−0.04	−0.01
Std of the difference		0.05	0.03	0.03	0.04	0.07	0.01	0.00
6140	2179.75	0.45	0.55	0.40	0.41	0.07	0.04	0.01
6143	2180.50	0.02	0.56	0.33	0.42	0.12	0.11	0.00
Difference		0.43	−0.02	0.07	−0.01	−0.05	−0.07	0.01
Std of the difference		0.07	0.02	0.02	0.03	0.04	0.01	0.00

Application to four years of Aqua/AIRS and MetOp-A/IASI

T. Thonat et al.

Table 3. Mean (upper line) and standard deviation (lower line) of the surface transmission (τ_s) and sensitivities of AIRS 2333 and IASI 7428 channels used to estimate surface temperature.

Channels	Wave nb (cm^{-1})	τ_s	ε_s 0.05	T_s 1 K	T 1 K	H_2O 20 %	CO_2 1 %	O_3 20 %	N_2O 2 %	CO 10 %	CH_4 10 %
AIRS 2333	2616.38	0.97	1.11	0.98	0.02	0.02	0.00	–	–	–	–
		0.03	0.06	0.01	0.01	0.03	0.00	–	–	–	–
IASI 7428	2501.75	0.90	1.01	0.92	0.07	0.01	0.00	–	–	–	–
		0.01	0.08	0.01	0.01	0.02	0.00	–	–	–	–

Table 4. Difference (in K) between simulated AIRS and IASI BT in clear-sky and BT with biomass burning aerosols, and corresponding perturbation of retrieved CO, for different altitudes, for the channels selected to retrieve CO.

Channels	Wave nb (cm^{-1})	Altitude (km)										
		0.25	0.75	1.24	1.72	2.33	3.11	3.90	4.66	5.39	6.08	6.74
AIRS												
1867	2183.31	0.01	0.01	0.02	0.03	0.05	0.07	0.10	0.12	0.13	0.15	0.16
1876	2191.50	0.01	0.01	0.02	0.03	0.05	0.07	0.09	0.11	0.13	0.15	0.16
1874	2189.67	0.00	0.01	0.02	0.03	0.04	0.07	0.09	0.11	0.13	0.14	0.16
1873	2188.76	0.01	0.01	0.02	0.03	0.05	0.07	0.09	0.11	0.13	0.15	0.16
1874	2189.67	0.00	0.01	0.02	0.03	0.04	0.07	0.09	0.11	0.13	0.14	0.16
1877	2180.50	0.01	0.01	0.02	0.03	0.05	0.07	0.09	0.11	0.13	0.15	0.16
ΔCO (ppbv)		−0.01	−0.03	−0.05	−0.07	−0.10	−0.13	−0.14	−0.14	−0.12	−0.10	−0.07
IASI												
6084	2165.75	0.01	0.02	0.03	0.04	0.06	0.08	0.10	0.12	0.14	0.15	0.16
6129	2177.00	0.01	0.02	0.03	0.04	0.06	0.08	0.10	0.12	0.14	0.16	0.17
6126	2176.25	0.01	0.01	0.02	0.03	0.05	0.07	0.09	0.11	0.13	0.15	0.16
6138	2179.25	0.01	0.01	0.02	0.04	0.05	0.08	0.10	0.12	0.14	0.15	0.17
6140	2179.75	0.01	0.01	0.02	0.04	0.05	0.07	0.10	0.12	0.13	0.15	0.16
6143	2180.50	0.01	0.01	0.02	0.04	0.05	0.08	0.10	0.12	0.14	0.15	0.16
ΔCO (ppbv)		0.00	−0.01	−0.02	−0.03	−0.04	−0.06	−0.08	−0.09	−0.09	−0.09	−0.08

Table 5. Same as Table 4 for dust aerosols.

Channels	Wave nb (cm^{-1})	Altitude (km)										
		0.25	0.75	1.24	1.72	2.33	3.11	3.90	4.66	5.39	6.08	6.74
AIRS												
1867	2183.31	0.09	0.13	0.18	0.24	0.31	0.41	0.52	0.61	0.69	0.76	0.82
1876	2191.50	0.09	0.13	0.18	0.24	0.31	0.41	0.51	0.60	0.68	0.74	0.80
1874	2189.67	0.07	0.10	0.15	0.20	0.28	0.38	0.48	0.57	0.66	0.73	0.79
1873	2188.76	0.08	0.11	0.16	0.22	0.29	0.39	0.50	0.59	0.67	0.74	0.80
1874	2189.67	0.07	0.10	0.15	0.20	0.28	0.38	0.48	0.57	0.66	0.73	0.79
1877	2180.50	0.07	0.11	0.16	0.22	0.30	0.40	0.50	0.60	0.67	0.74	0.80
ΔCO (ppbv)		−0.16	−0.28	−0.43	−0.58	−0.71	−0.81	−0.78	−0.64	−0.44	−0.21	0.04
IASI												
6084	2165.75	0.14	0.18	0.23	0.29	0.36	0.45	0.54	0.62	0.68	0.74	0.78
6129	2177.00	0.13	0.18	0.23	0.29	0.36	0.46	0.55	0.64	0.71	0.77	0.82
6126	2176.25	0.10	0.14	0.18	0.24	0.31	0.41	0.50	0.59	0.67	0.74	0.80
6138	2179.25	0.09	0.14	0.19	0.25	0.34	0.44	0.54	0.63	0.70	0.76	0.81
6140	2179.75	0.10	0.14	0.19	0.25	0.32	0.42	0.52	0.61	0.68	0.75	0.80
6143	2180.50	0.10	0.14	0.19	0.25	0.32	0.42	0.52	0.61	0.68	0.75	0.80
ΔCO (ppbv)		0.05	−0.02	−0.01	−0.19	−0.30	−0.40	−0.45	−0.46	−0.43	−0.39	−0.33

Table 6. Mean (upper line) and standard deviations (lower line) of variations of AIRS and IASI CO induced by random variations of T_s (3 K), T (2 K), H_2O (10 %) and N_2O (2 %), in January and July 2008.

	T_s	T	H_2O	N_2O	4 Variables
AIRS					
2008-01	0.04	−0.02	−0.02	0.00	0.01
	1.28	1.24	1.61	0.28	2.38
2008-07	0.10	0.01	−0.01	0.00	0.10
	2.12	1.16	1.02	0.26	2.62
IASI					
2008-01	−0.05	−0.07	0.00	0.01	−0.10
	0.89	1.64	0.58	1.33	2.35
2008-07	−0.02	−0.04	0.00	−0.01	−0.07
	0.85	2.00	0.37	1.32	2.57

Table 7. Comparisons between CARIBIC and AIRS (upper part) and IASI (lower part). Average of the difference CARIBIC-AIRS or CARIBIC-IASI, standard deviation of the difference, linear regression coefficient, relative difference and number of collocated $1° \times 1°$ grid cells, over the period (July 2007–June 2011) (60 flights for AIRS and 57 flights for IASI), for each season and for the whole year.

	CARIBIC-Sounder (ppbv)	Std (ppbv)	R	Rel. diff. (%)	Nb. of grid cells
AIRS					
Whole year	6.1	18.4	1.21	4.92	483
DJF	10.1	20.3	1.74	7.74	125
MAM	6.4	24.6	0.91	4.25	120
JJA	3.0	11.5	0.64	3.47	143
SON	5.3	13.7	1.34	1.25	95
IASI					
Whole year	3.6	13.0	1.08	3.42	478
DJF	1.1	11.4	0.82	1.06	60
MAM	3.4	20.8	1.63	0.92	95
JJA	5.7	9.0	1.46	6.66	140
SON	2.9	10.5	0.95	3.02	183
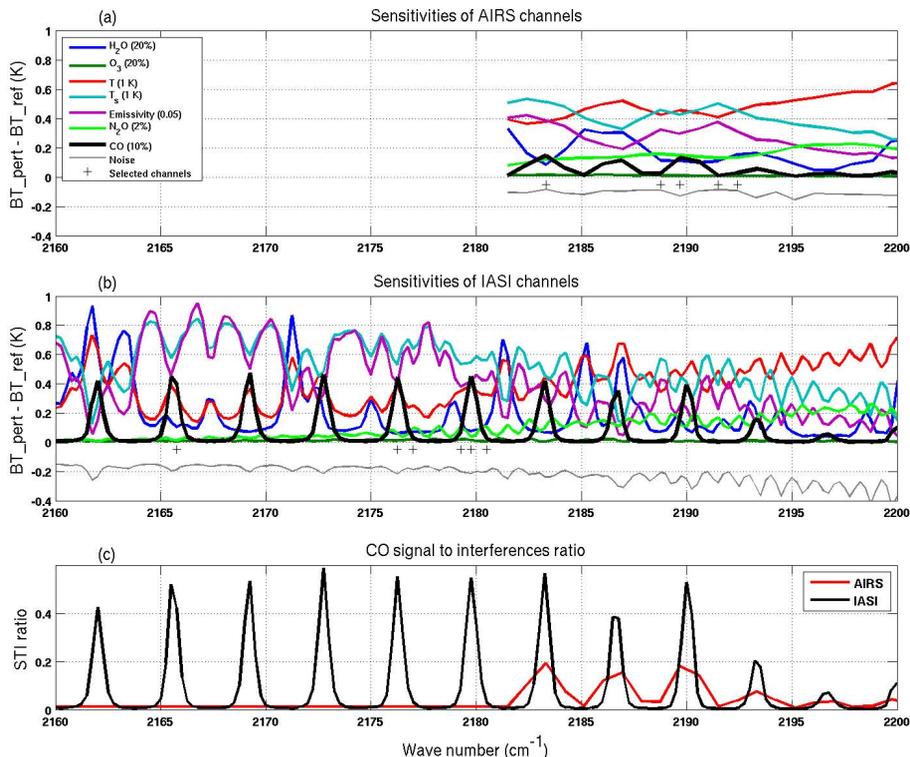
Fig. 1. Sensitivities of **(a)** AIRS channels and **(b)** IASI channels to variations of 10 % CO (black), 0.05 emissivity (magenta), 1 K surface temperature (cyan), 1 K temperature (red), 20 % H_2O (blue), 2 % N_2O (pale green) and 20 % O_3 (dark green). The grey line is the radiometric noise, multiplied by -1 for clarity. The crosses indicates the position of the selected channels. **(c)** CO signal to interferences (STI) ratio for AIRS (red) and IASI (black). The sensitivities are computed with 4A and averaged over the 872 TIGR tropical atmospheric situations. AIRS spectral domain does not cover the CO absorption band before 2181.5 cm^{-1}.
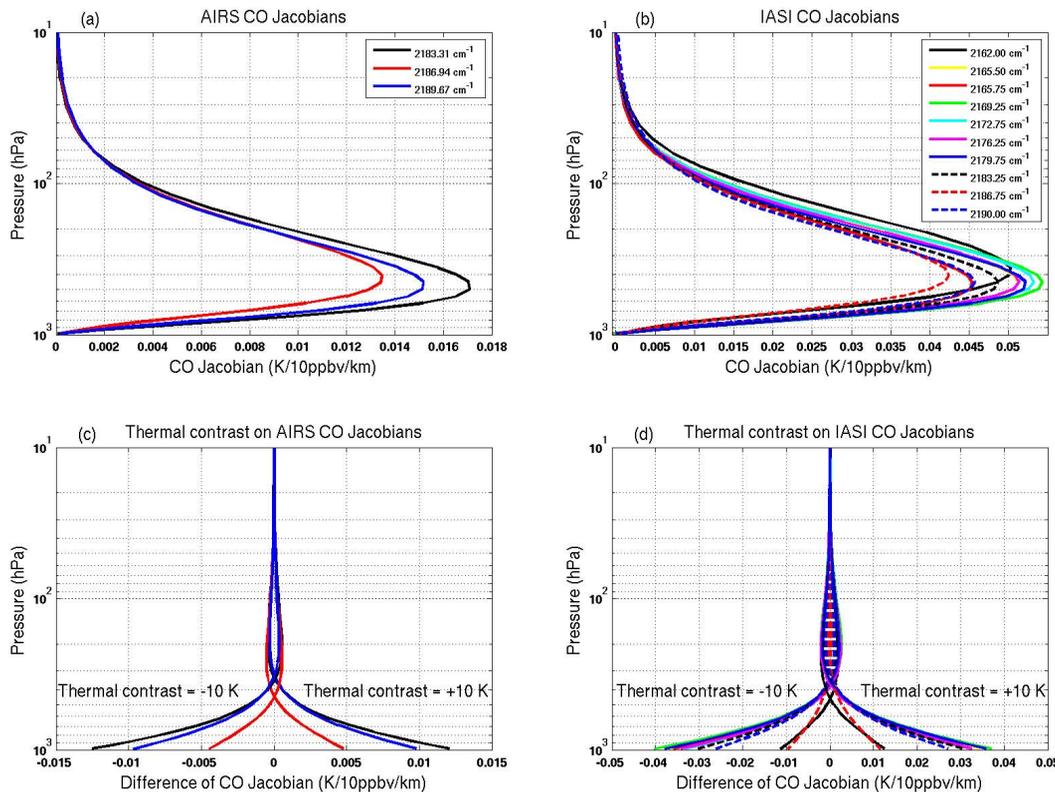
Fig. 2. CO Jacobians (K/10 ppbv/km) corresponding to a variation of 10 ppbv for **(a)** AIRS and **(b)** IASI. Effect of thermal contrasts of −10 and +10 K on **(c)** AIRS and **(d)** IASI CO Jacobians. The Jacobians are computed with 4A and averaged over the 872 TIGR tropical atmospheric situations. The channels represented here are those with the highest sensitivity to CO (see Fig. 1a and b).
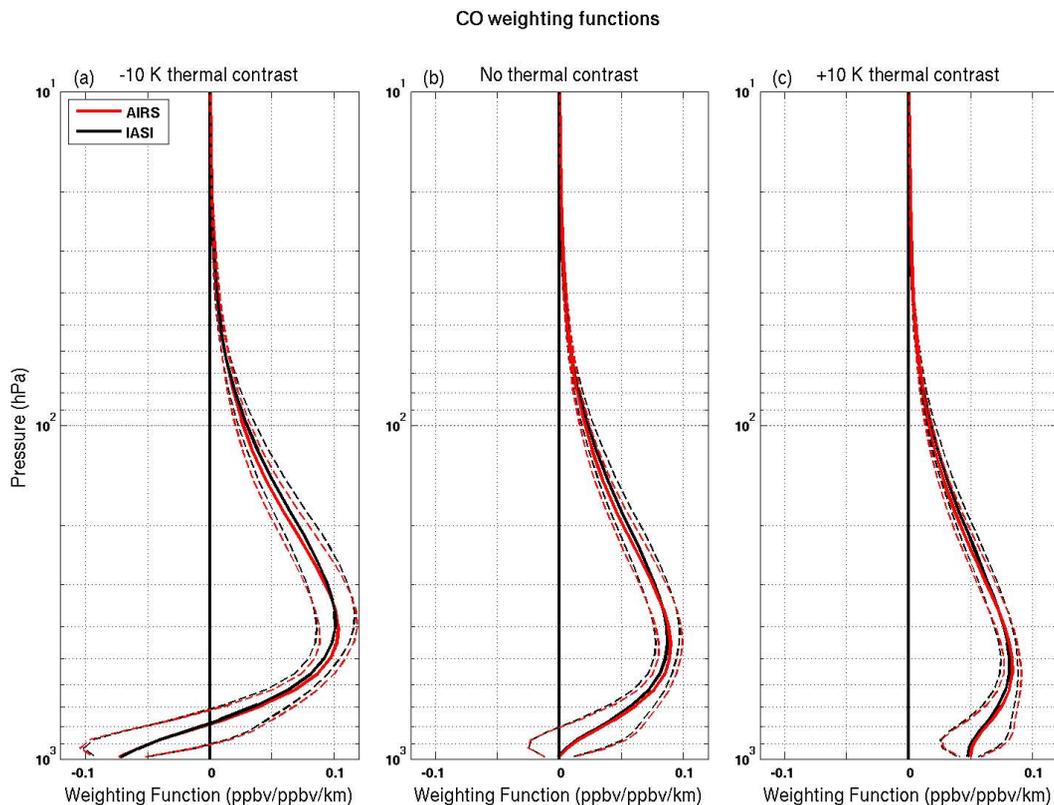
Fig. 3. Mean (solid lines) ± standard deviation (dashed lines) of the weighting functions of AIRS (red) and IASI (black), with **(a)** a −10 K thermal contrast, **(b)** a null thermal contrast, and **(c)** a +10 K thermal contrast (right). The weighting functions are computed over the 872 TIGR tropical atmospheric situations.
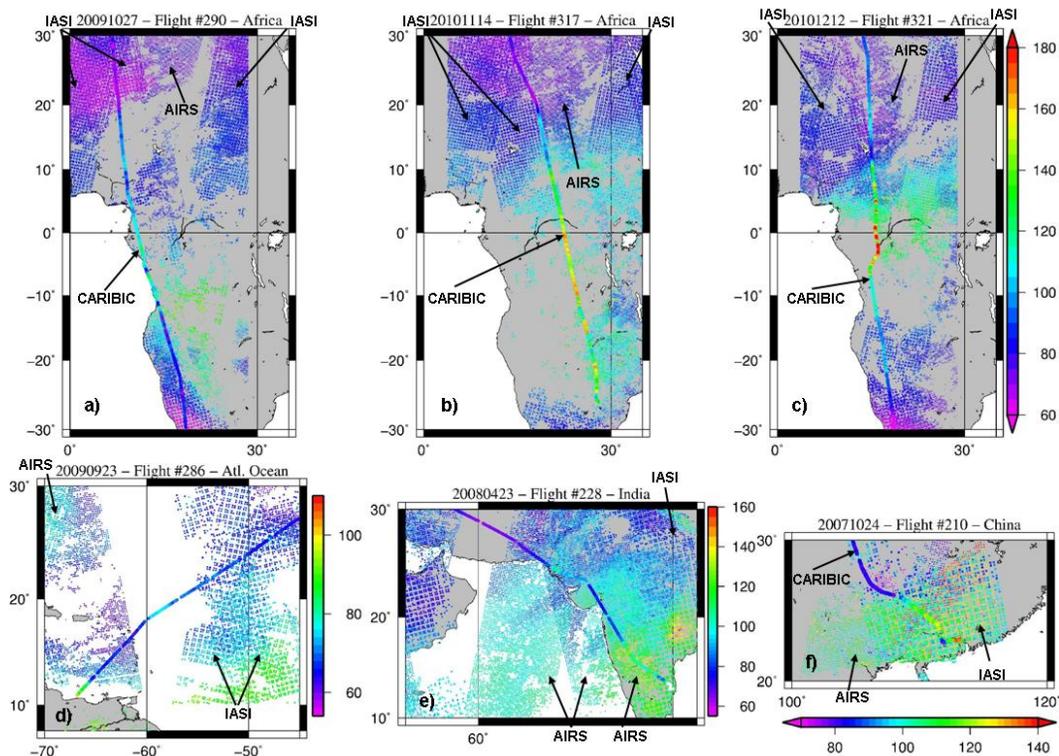
Fig. 4. CO measured by CARIBIC aircrafts at ∼10 km altitude for 6 flights over Africa **(a–c)**, the Atlantic Ocean **(d)**, India **(e)** and China **(f)**, and corresponding AIRS and IASI mid-tropospheric content of CO (ppbv).
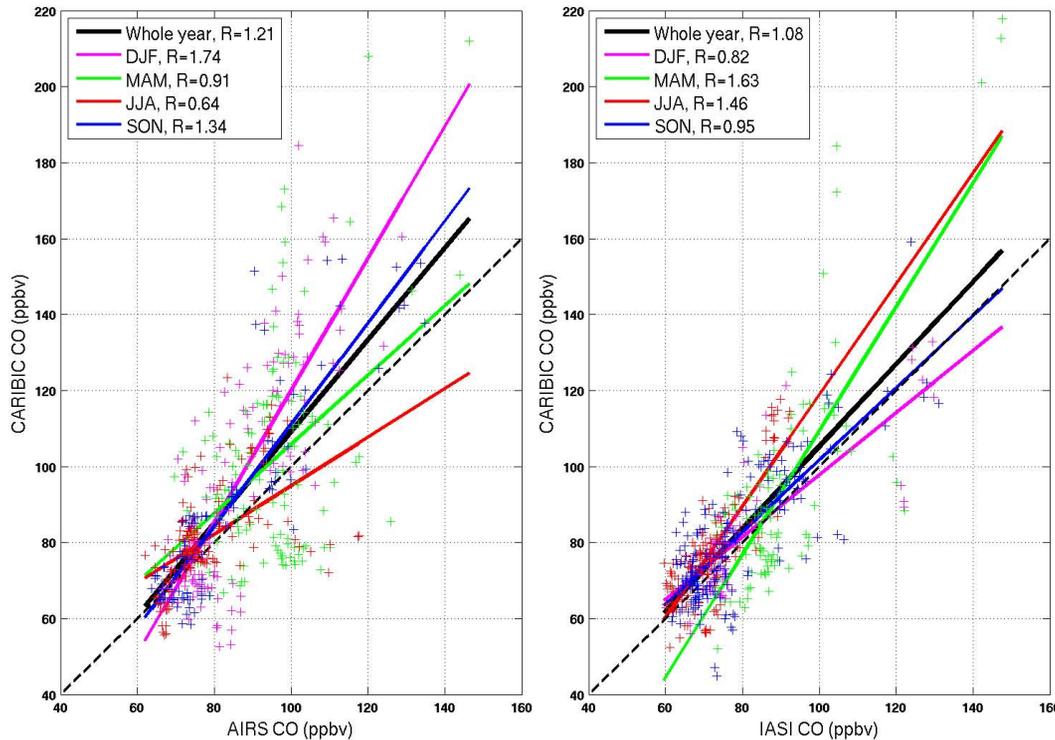
Fig. 5. Scatter plots of 1° × 1° averaged CARIBIC and AIRS (left panel) and IASI (right panel) CO. The coloured lines represent the linear regression between the data for each season (pink: December-January-February, green: March-April-May, red: June-July-August, blue: September-October-November) and the black line for all seasons. The black dashed line gives the 1:1 line.
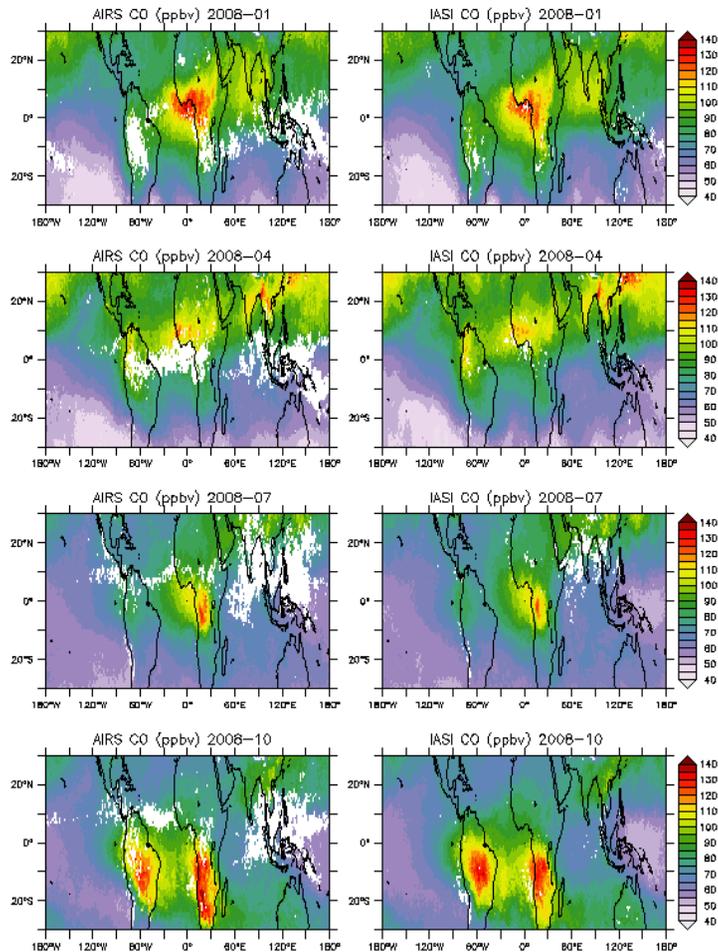
Fig. 6. AIRS (left panels) and IASI (right panels) monthly average mid-tropospheric CO (ppbv) for January, April, July and October 2008. Blank zones correspond to persistent cloudiness.
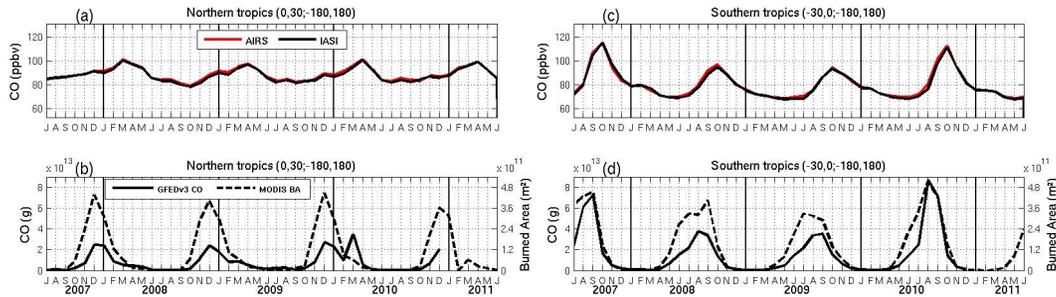
Fig. 7. (a) Time series of AIRS (red) and IASI (black) CO over land, for the northern tropics. **(b)** Time series of GFEDv3 CO emissions (solid line) and MODIS Burned Area (dashed line) for the northern tropics. **(c)** and **(d)** same as **(a)** and **(b)**, respectively, for the southern tropics.
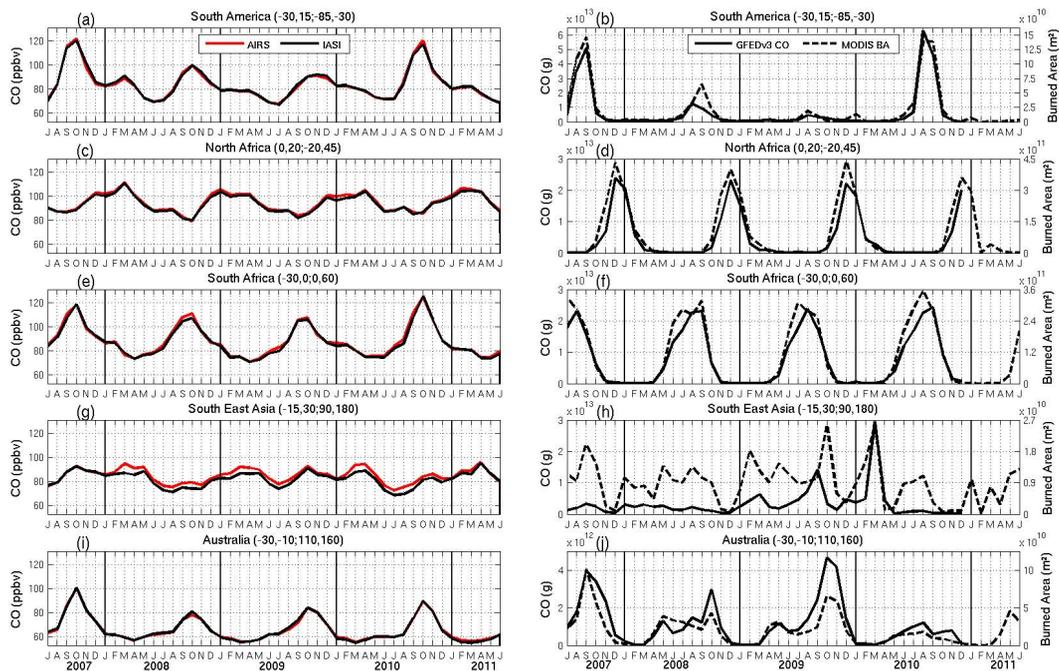
Fig. 8. Same as Fig. 7 for 5 tropical areas: South America **(a, b)**, North Africa **(c, d)**, South Africa **(e, f)**, South East Asia **(g, h)** and Australia **(i, j)**. Coordinates of the areas are given as follow: (latitude S, latitude N; longitude W, longitude E).
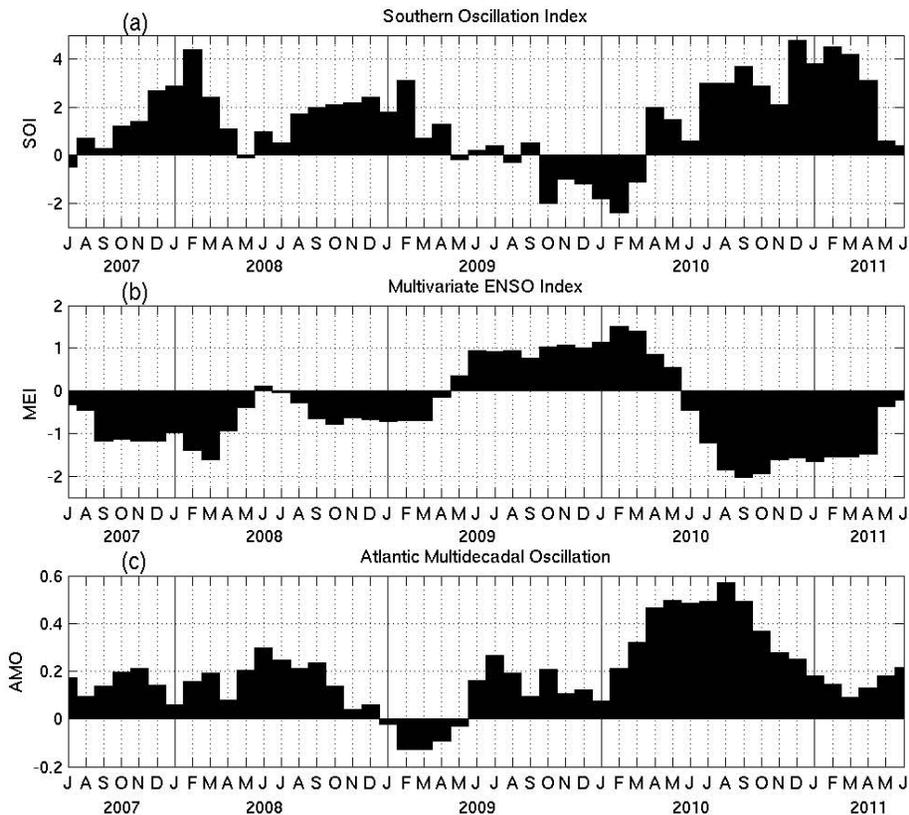
Fig. 9. Climate indexes for the period July 2007–June 2011. **(a)** Southern Oscillation Index. **(b)** Multivariate ENSO Index. **(c)** Atlantic Multidecadal Oscillation. The data come from the ESRL/NOAA.

Title Page

Abstract | Introduction

Conclusions | References

Tables | Figures

◄ | ►►

◄ | ►

Back | Close

Full Screen / Esc

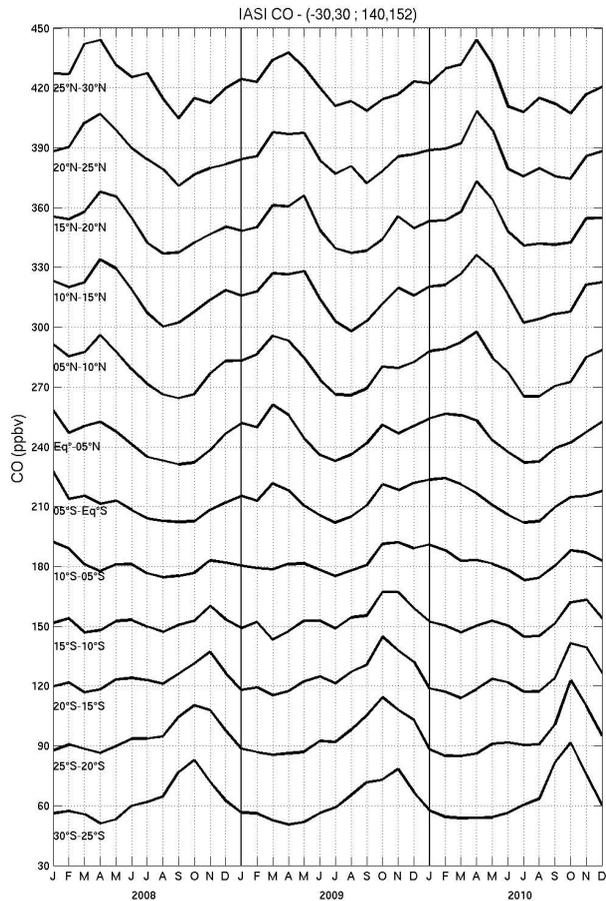Printer-friendly Version

Interactive Discussion

Fig. 10. IASI CO (ppbv) from 30° N to 30° S averaged over 140:152 E for 12 latitudinal bands of 5° each. The scale corresponds to the (30° S, 25° S) band; 30 ppbv is added to each following latitudinal band.